On the Influence of Metal Chucks in Wideband On-Wafer Measurements

Gia Ngoc Phung and Uwe Arz
Physikalisch-Technische Bundesanstalt (PTB), Bundesallee 100, 38116 Braunschweig, Germany

***Abstract*—On-wafer measurements are essential for the characterization of electronic devices at millimeter-wave frequencies. They have been known as challenging and ambitious containing a lot of parasitic effects. While a lot of investigations have been performed for on-wafer measurements of coplanar waveguides (CPW) placed on ceramic chucks, the parasitic effects related to the influence of metal chucks have not been fully investigated yet. This paper demonstrates a systematic study of the metal chuck in conjunction with the parasitic probe effects using two different probe types in mTRL-calibrated CPW measurements through a thorough field analysis.**

***Index Terms*—calibration, coplanar waveguides, on-wafer, probes.**

I. Introduction

On-wafer measurements are an underpinning technology for the characterization of electronic devices at millimeter-wave frequencies. With emerging applications in communications and electronics technologies – e.g. 5th Generation mobile networks (5G), Internet of Things (IoT), Connected and Autonomous Vehicles (CAVs), on-wafer measurements are becoming more and more important. They have been known to reveal a lot of parasitic effects stemming from probe effects, multimode propagation, crosstalk between adjacent structures and radiation effects. In recent years, the parasitic effects on coplanar waveguides (CPW) measured on ceramic chucks have been investigated in the framework of the PlanarCal project [1]. The parasitic effects are related to different effects such as e.g. multimode propagation ([2], [3] and [4]), crosstalk effects and the influence of microwave probes ([5], [6] and [7]). While a number of investigations have been performed for conventional coplanar waveguides measured on ceramic chuck, the parasitic effects related to CPWs measurements on metal chuck are not yet fully clarified.

With this motivation, this paper addresses the influence of metal chucks in conjunction with the impact of probe effects in mTRL-calibrated CPW measurements. Starting with a measurement example, this paper presents a systematic study discussing the influence of metal chuck in CPW measurements for two different probe types. Furthermore, comparisons to the ceramic chuck (with a thickness of around 8 mm) which represents presently the most preferable solution for high-frequency coplanar characterization will be made. For comparison purposes, the measurements were performed with probes from different vendors (MPI and GGB)[1] with a 100 µm pitch. For the electromagnetic simulations, CST Studio Suite from Dassault Systemes was applied [8]. The reference plane

[1]We use brand names only to better specify the experimental conditions. PTB does not endorse commercial products. Other products may work as well or better.

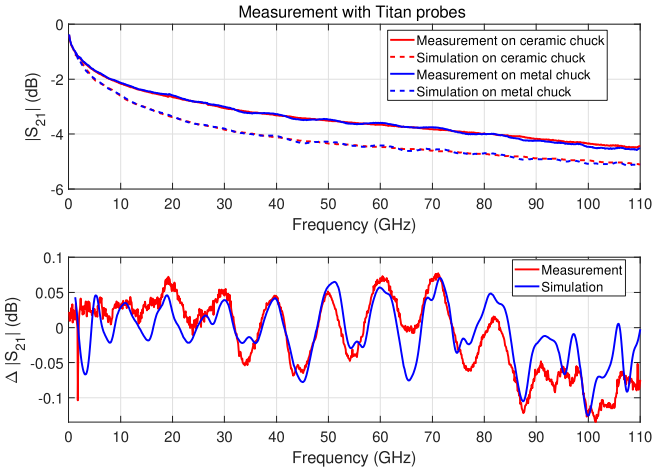

Fig. 1. Measurement and em simulation of the CPW with l = 7400 µm with Titan probes on different chuck materials: Transmission coefficient $|S_{21}|$ and difference $\Delta|S_{21}|$ between transmission on metal and ceramic chuck.

of the calibration was shifted to the probe tips for all the comparisons. All simulated and measured data presented here were calibrated with a mTRL algorithm according to [9] which is commonly accepted as one of the most accurate calibration algorithms. The calibration kit uses a short as reflect, a 400 µm long CPW line as thru and a selection of seven additional lines with lengths between 500 and 11400 µm. The measured CPW structures were manufactured on a fused silica substrate (ϵ_r = 3.78) and have been investigated also in [10]. The common parameters of the CPW cross section are the signal width w = 62 µm, the gap width s = 6 µm, the metal ground width w_g = 250 µm, the metal thickness t = 0.534 µm, and the substrate height h = 254 µm.

II. Measurement and Simulation Results

Fig. 1 shows the magnitude of the transmission coefficient S_{21} of the CPW with l = 7400 µm for both chuck conditions (ceramic and metal chuck) simulated and measured with Titan probes. For comparison purposes the relative difference $\Delta|S_{21}|$ is plotted, which is defined as follows:

$$\Delta|S_{21}| = |S_{21,metal}| - |S_{21,ceramic}| \quad (1)$$

At first sight, one can observe a reasonable agreement between the em simulation of $|S_{21}|$ and measurement. Overall, there is a slight shift between the measured and simulated data due to the incomplete knowledge of cross-section and material parameters. Comparing $\Delta|S_{21}|$ on the other hand, a better agreement between the em simulation and measurements can be detected. When comparing the different chuck conditions,

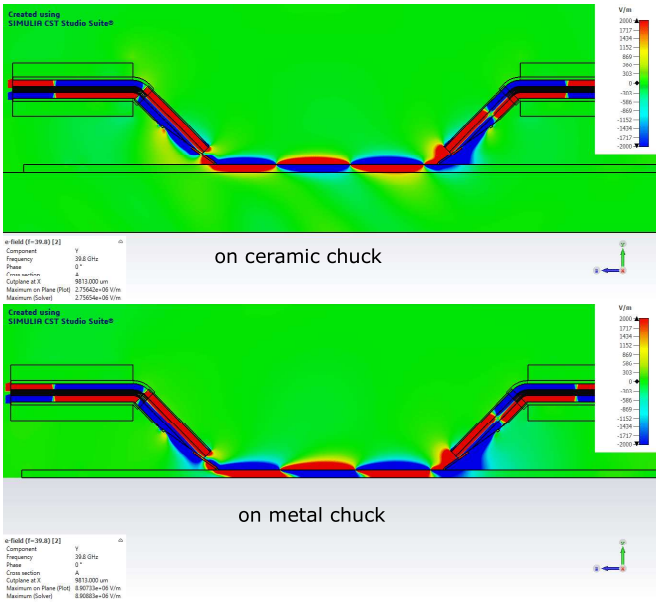

Fig. 2. Cross-sectional view: simulated vertical electric field component of the CPW with l = 7400 µm with Titan probes on different chucks at local maximum $\Delta|S_{21}|$ i.e. f = 39.8 GHz.

the metal and ceramic chuck, one can clearly state that the metal chuck case reveals strong ripples in $|S_{21}|$ whereas the ceramic chuck case shows an almost ideal smooth curve within the investigated frequency range. To understand this behavior, the cross-sectional view of the em-simulated vertical electric field component is illustrated for the CPW with l = 7400 µm placed on the ceramic and metal chuck (see Fig. 2).

As expected for the ceramic chuck, a single CPW mode propagation can be observed. The field plots for the metal chuck on the other hand show the propagation and superposition of two modes, i.e. the expected CPW mode and an additional parallel plate line (PPL) mode. The PPL mode is more concentrated inside the substrate therefore the phase constant is in general larger than that of the CPW mode ($\beta_{\mathrm{PPL}} > \beta_{\mathrm{CPW}}$). Thus, the interaction and superposition of the two modes leads to phase distortions. The resonance effects detected in the measurement results (Fig. 1) are related to the destructive interference of the two modes. The PPL mode is propagating along the CPW line. Moreover, the propagation path of the PPL mode is also determined by the regions around probe needles and the coaxial extensions.

Complementing the results of Fig. 1, we performed additional simulations and measurements with probes from another vendor (GGB), which are plotted in Fig. 3.

In Fig. 4 a comparison between the measurements with the two different probe types is made. At first sight, the measurements performed on ceramic chuck show a smooth behavior independent of which probes are applied. In case of the metal chuck, the situation changes. Obviously, the metal chuck initiates ripples and the ripples reveal a different behavior due to the different probe geometries. Especially, the

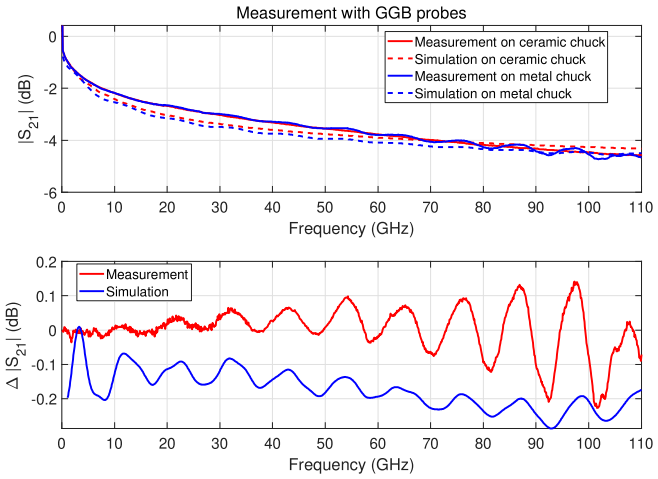

Fig. 3. Measurement and em simulation of the CPW with l = 7400 µm with GGB probes on different chuck materials: Transmission coefficient $|S_{21}|$ and difference $\Delta|S_{21}|$ between transmission on metal and ceramic chuck.

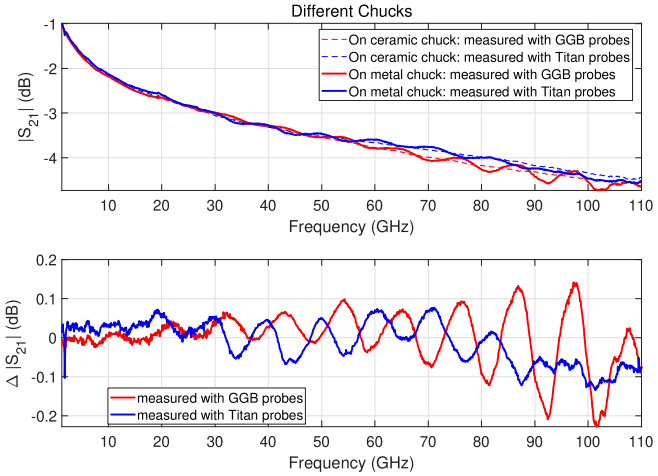

Fig. 4. Measurement of the CPW with l = 7400 µm with different probes and on different chuck materials: Transmission coefficient $|S_{21}|$ and difference $\Delta|S_{21}|$ between transmission on metal and ceramic chuck.

shape, position and strength of the ripples differ strongly and depend on the probe types used, as can be clearly seen from the difference plot $\Delta|S_{21}|$ in Fig. 4. The reason for this can be traced back to the propagation path of the PPL mode. The PPL mode is not only propagating along the CPW line, but is also supported by the probe needles and transferred into the air region surrounded by the absorber enclosing the coaxial line of the probe and the calibration substrate. Thus, different probe constructions lead to different probe coupling to the PPL mode.

The fields shown in Fig. 5 support this statement. Depending on the probe types used the fields around the probe needles and the field coupling to the PPL mode differs. Compared to the GGB probes, the Titan probes have a steeper probe angle of around 45°. The GGB probes are oriented more parallel to the calibration substrate with a probe angle of around 25°...30°.

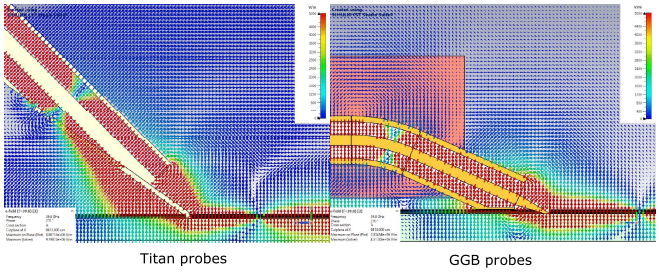

Fig. 5. Cross-sectional view of the electric field vectors around the probe needle and tip regions at f = 39.8 GHz.

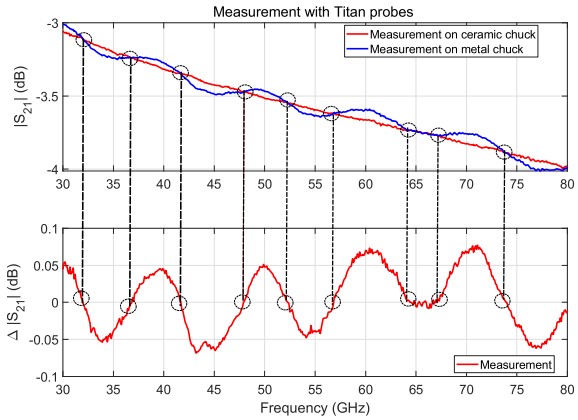

Fig. 6. Zoomed-in-view of the measurement results of Fig. 1 in the frequency range between f = 30...80 GHz where the ripples can be seen.

Thus, the coupling to the PPL mode for the GGB probes is also more pronounced. This explains why the strength of the ripples in $\Delta|S_{21}|$ is also more pronounced for the GGB probes (Fig. 4).

III. Discussion : Comparison to the Ceramic Chuck

So far, our investigations have demonstrated that the parasitic ripples detected in the measurement results are related to the superposition of the CPW mode with the PPL mode and in addition to the parasitic probe effects. Another important question is whether, at least for some frequencies, the quality of the measurements on the metal chuck and on the ceramic chuck can be considered equivalent.

Compared to the ceramic case, interestingly, there are some intersection points between the metal chuck and ceramic chuck. This behavior is more visible when we compare the measurements in the frequency range between f = 30...80 GHz where the ripples can be better seen.

Fig. 6 presents a zoomed-in-view of the measurements in Fig. 1 for the Titan probes whereas Fig. 7 shows the corresponding results for the GGB probes. It is important to note that the intersection points occur at irregular intervals. At the intersection points the corresponding difference $\Delta|S_{21}|$ reaches zero. This statement is valid for the two different probe types used, i.e. the Titan probes and GGB probes.

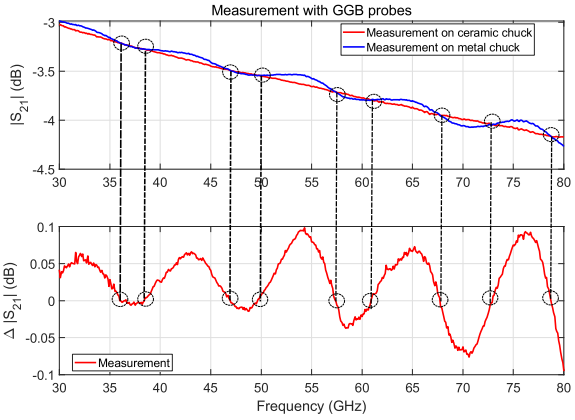

Fig. 7. Zoomed-in-view of the measurement results of Fig. 3 in the frequency range between f = 30...80 GHz where the ripples can be seen.

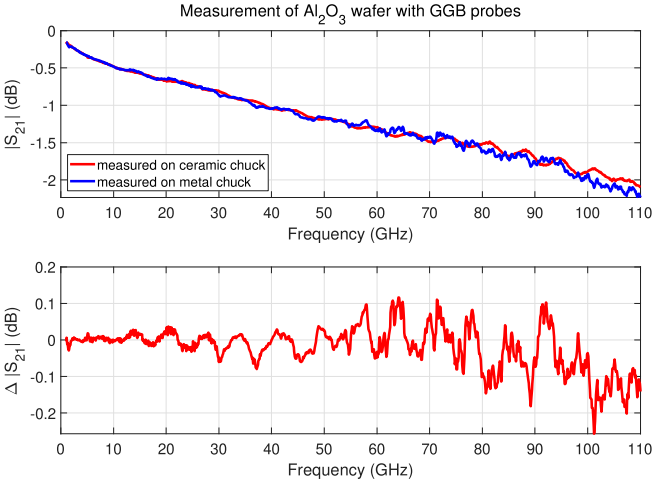

Fig. 8. Measurement of the CPW with l = 7400 µm on an alumina substrate with GGB probes on different chuck materials: Transmission coefficient $|S_{21}|$ and difference $\Delta|S_{21}|$ between transmission on metal and ceramic chuck.

So far, we have performed the systematic study based on the measurements and simulations by using an almost ideal case on fused silica with a relatively low permittivity. The question is how the situation changes when larger permittivities are used for the substrate material. Therefore, CPWs manufactured on an alumina substrate (ϵ_r = 9.7) were also investigated (see also [11]). The same CPW length l = 7400 µm is also available on this wafer. For the comparison, measurements performed on metal and ceramic chuck are repeated for the alumina wafer. Due to the larger substrate permittivity of ϵ_r = 9.7 compared to the ceramic chuck permittivity of ϵ_r = 6.5, this example is expected to also support surface wave propagation.

Obviously, the measurements of Fig. 8 show an interesting behavior. Here, the ceramic chuck also reveals a wavy curve behavior and does not represent an ideal case any more. The metal chuck on the other hand not only supports stronger ripples but also a noisy curve behavior over the whole frequency range.

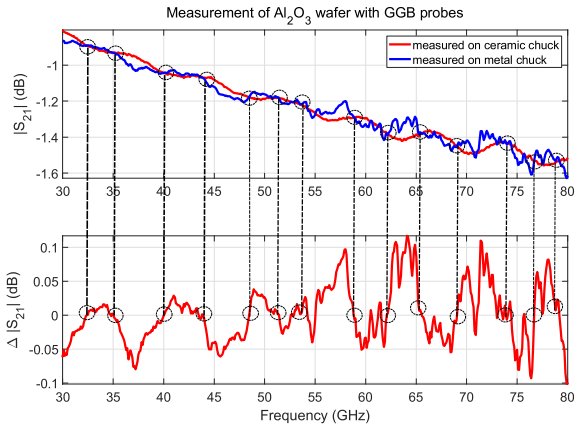

Fig. 9. Zoomed-in-view of the measurement results of Fig. 8 in the frequency range between f = 30...80 GHz where the ripples can be seen.

Comparing the zoomed-in-view of the measurement results in Fig. 9, as expected the intersection points also occur at irregular intervals. At these points $\Delta|S_{21}|$ also reaches zero. Compared to the fused silica case, the irregularities of the intersection points are significantly larger, making a prediction much more difficult. It is less clear to which physical effects the observed behavior can be traced back.

IV. Conclusion

In this paper the influence of the metal chuck in conjunction with the parasitic probe effects in CPW measurements using two different probe types is studied. This paper explains how the metal chuck deteriorates the mTRL-calibrated measurements. Summarizing the results deduced from comparisons to the ceramic chuck case, the metal chuck initiates ripples which depend on the CPW line length and the probe properties. Currently, research is in progress for developing analytical expressions which will help to better predict the occurrence of ripples in CB-CPWs including the parasitic probe effects.

Acknowledgment

The authors acknowledge support by the European Metrology Programme for Innovation and Research (EMPIR) Projects 14IND02 PlanarCal and 18SIB09 TEMMT. Both projects (14IND02 and 18SIB09) have received funding from the EMPIR programme co-financed by the Participating States and from the European Union's Horizon 2020 research and innovation programme.

The authors are also grateful to Rohde & Schwarz for manufacturing the calibration substrates and to Dr. Andrej Rumiantsev for providing us the CST model of the Titan probes.

References

[1] European Metrology Programme for Innovation and Research JRP Number 14IND02, "Microwave Measurements for Planar Circuits and Components." https://planarcal.ptb.de.

[2] M. Tsuji, H. Shigesawa, and A. A. Oliner, "New Surface-Wave-Like Mode on CPWs of Infinite Width and its Role in Explaining the Leakage Cancellation Effect," in *1992 IEEE MTT-S Microwave Symposium Digest*, 1992, pp. 495–498 vol.1.

[3] H. Shigesawa, M. Tsuji, and A. A. Oliner, "A New Mode-Coupling Effect on Coplanar Waveguides of Finite Width," in *IEEE International Digest on Microwave Symposium*, 1990, pp. 1063–1066 vol.3.

[4] E. M. Godshalk, "Surface Wave Phenomenon in Wafer Probing Environments," in *40th ARFTG Conference Digest*, vol. 22, 1992, pp. 10–19.

[5] G. N. Phung, F. J. Schmückle, R. Doerner, B. Kähne, T. Fritzsch, U. Arz, and W. Heinrich, "Influence of Microwave Probes on Calibrated On-Wafer Measurements," *IEEE Transactions on Microwave Theory and Techniques*, vol. 67, no. 5, pp. 1892–1900, 2019.

[6] S. Fregonese, M. De matos, M. Deng, M. Potereau, C. Ayela, K. Aufinger, and T. Zimmer, "On-Wafer Characterization of Silicon Transistors Up To 500 GHz and Analysis of Measurement Discontinuities Between the Frequency Bands," *IEEE Transactions on Microwave Theory and Techniques*, vol. 66, no. 7, pp. 3332–3341, 2018.

[7] C. Yadav, M. Deng, S. Fregonese, M. Cabbia, M. De Matos, B. Plano, and T. Zimmer, "Importance and Requirement of Frequency Band Specific RF Probes EM Models in Sub-THz and THz Measurements up to 500 GHz," *IEEE Transactions on Terahertz Science and Technology*, vol. 10, no. 5, pp. 558–563, 2020.

[8] "CST Studio Suite," 2020. [Online]. Available: https://www.3ds.com/products-services/simulia/products/cst-studio-suite/

[9] R. B. Marks, "A Multiline Method of Network Analyzer Calibration," *IEEE Trans. on Microwave Theory and Techniques*, vol. 39, no. 7, pp. 1205–1215, 1991.

[10] U. Arz, K. Kuhlmann, T. Dziomba, G. Hechtfischer, G. N. Phung, F. J. Schmückle, and W. Heinrich, "Traceable Coplanar Waveguide Calibrations on Fused Silica Substrates up to 110 GHz," *IEEE Transactions on Microwave Theory and Techniques*, vol. 67, no. 6, pp. 2423–2432, 2019.

[11] G. N. Phung, F. J. Schmückle, R. Doerner, W. Heinrich, T. Probst, and U. Arz, "Effects Degrading Accuracy of CPW mTRL Calibration at W Band," in *2018 IEEE/MTT-S International Microwave Symposium - IMS*, 2018, pp. 1296–1299.